# Interface Passivation of Inverted Perovskite Solar Cells by Dye Molecules

*Yifang Qi[a], David Ndaleh[b], William E. Meador[b], Jared H. Delcamp[b], Glake Hill [a], Nihar Ranjan Pradhan[a], and Qilin Dai[a*]*

a Department of Chemistry, Physics, and Atmospheric Sciences, Jackson State University, Jackson, MS, 39217, United States

b Department of Chemistry and Biochemistry, University of Mississippi, Oxford, MS, 38677, United States

* Corresponding author: Q. Dai, Email: *qilin.dai@jsums.edu*

ABSTRACT

The interface between $PC_{61}BM$ and an electrode has a critical effect on the performance of inverted perovskite solar cells (PSCs). Three organic cationic cyanine dye molecules with different highest occupied molecular orbital (HOMO) and lowest unoccupied molecular orbital (LUMO) states are designed to passivate the $PC_{61}BM$ and Ag electrode interface to improve PSC device performance. The effects of energy level alignment and the interfacial charge transfer resistance on the device performance are compared and studied. The dye interface passivation layer significantly reduces charge recombination. Moreover, dye $ClO_4^-$ anions associated with the dye molecules improve the charge extraction and charge transport in the devices. Reduced interface charge recombination and improved charge transport are confirmed by photoluminescence (PL), time-resolved photoluminescence (TRPL), electrochemical impedance spectra (EIS), and charge-only device performance studies. The PSCs with one of the dyes as an interface passivation layer show an optimized power conversion efficiency (PCE) of 19.14% with an open-circuit voltage (Voc) of 1.09V, a short-circuit current density (Jsc) of 22.87 $mA/cm^2$, and an fill factor (FF) of 76.81%. The devices maintain over 90 % of the initial PCE for 120 h of storage under ambient environment (25℃ and 30±5 % RH). The use of small dye molecules as an interface passivation layer to reduce charge recombination in PSCs represents a paradigm for improving the performance and stability of PSCs.

KEYWORDS: Inverted Perovskite, Cyanine dye, Charge transport, Interface, Stability

## 1. INTRODUCTION

To date, the power conversion efficiency (PCE) of solution-processed hybrid organic/inorganic perovskite solar cells (PSCs) has reached 25.5 %[1]. PSCs are considered as exceptionally promising next-generation solar cells due to high PCEs, low-cost processing, and the potential for large scale manufacturing[2,3]. The high PCE of simply processed PSCs is more challenging to process comparable to silicon solar cells [4–6]. Most of the high PCE devices are based on the n-i-p structure with high-quality mesoporous and dense $TiO_2$ as an electron-transporting layer[7]. However, high-quality $TiO_2$ films require high temperatures over 400 ℃, which is time-consuming, restricts substrate choice, and adds complications to large scale manufacturing[8–10]. In comparison to the regular n-i-p structure, the inverted structure (p-i-n) PSCs show many advantages including low-temperature fabrication (~100 ℃), lightweight designs, low cost

materials and production, and low-hysteresis[11,12]. In addition, inverted PSCs are compatible with roll-to-roll production due to their high flexibility[13]. However, inverted PSCs still have some challenges. [6,6]-phenyl $C_{61}$-butyric acid methyl ester ($PC_{61}BM$) is the common electron transport layer in inverted PSCs, and the porous structure of $PC_{61}BM$ influences the charge extraction and transport in the devices. The interface between $PC_{61}BM$ and electrode has a critical effect on the device performance in terms of carrier extraction and recombination loss [14–16]. In addition, the interface also induces moisture, oxygen, and metal ion diffusion from the electrode into perovskite film[17]. Therefore, many strategies have been pursued toward passivation of the $PC_{61}BM$/electrode interface. Xiong *et al.* used Isatin and Isatin-Cl to passivate the interface between $PC_{61}BM$ and Ag to enhance charge transport, leading to improved efficiency and stability of PSCs [17]. Guarnera *et al.* introduced $Al_2O_3$ nanoparticles to the interface to prevent metal electrode migration, resulting in improved stability of PSCs[18]. Li *et al.* invoked 1-butyl-3-methylimidazolium tetrafluoroborate as an interface passivation layer between $PC_{61}BM$ and Ag electrode to reduce defect density[19].

Regarding the mechanism of the improved device performance by an interface passivation layer, some papers attributed it to the improved energy level alignment due to the high energy mismatch between $PC_{61}BM$ and the metal electrode[17,20]. Better energy level alignment can improve the charge transport in the devices[17,20]. Some research efforts show that device improvements are associated with improved interface contact[21–23]. Improved interface contact reduces the interface charge recombination, leading to improved device performance[21–23]. However, it is still not clear which mechanism is dominant since the device performance is always ascribed to the above two mechanisms simultaneously. Interface contact and energy level alignment are likely two critical factors affecting the device performance due to interface passivation layers. Determination of the dominant factor between the two is challenging. Thus, fundamental understanding of the improved device performance caused by the interface passivation layer is necessary for PSCs design and development toward higher PCEs.

In this work, three cationic cyanine dye molecules with $ClO_4^-$ ions as shown in the inset of Figure 1a are used to passivate the interface between $PC_{61}BM$ and metal electrode. The three dyes are designed to have HOMO and LUMO energy levels which are tunable for alignment of energy level between the $PC_{61}BM$, dye, and Ag electrode. The dye interface passivation layers can reduce charge recombination and metal ion migration. Moreover, the dye interface passivation layer between $PC_{61}BM$ and Ag can adjust the energy level alignment to reduce the energy barrier,

leading to enhanced charge transport in the PSC devices. The results show that interface contact is the major factor that affects the device performance since the two dyes with near identical energy levels and core structures show substantially different performances. The PSCs with a dye interface passivation layer exhibit a high PCE of 19.14% with a Voc of 1.09V, a Jsc of 22.87 mA/cm$^2$, and an FF of 76.81%. In addition, PSCs with the dye interface passivation layer show improved stability under the ambient environment (25℃ and 30±5 % RH). The devices maintain PCEs over 90 % of the initial PCE after 120 hours of storage.

## 2. EXPERMENT SECTION

### *2.1 Materials*

All chemicals were used as received without further treatment. Methylammonium iodide (MAI, 99.5 %) was purchased from Xi'an Polymer Light Technology Corporation (China). Poly[bis(4-phenyl) (2,4,6-trimethylphenyl) amine] (PTAA, >99 %) was obtained from Solaris Chem. (Canada). Lead iodide ($PbI_2$, 99 %) is purchased from TCI America. *N*,*N*-Dimethylformamide (DMF, anhydrous 99.8%), isopropanol (IPA, anhydrous 99.5%), chlorobenzene (CB, anhydrous 99.8%), and [6,6]-phenyl $C_{61}$-butyric acid methyl ester ($PC_{61}BM$, 99.5%) were purchased from Sigma-Aldrich (USA). Dimethyl sulfoxide (DMSO, 99.8%) was purchased from Alfa Aesar. ITO coated glass substrates (7~9 Ω/cm$^2$) were purchased from Advanced Election Technology Co.,Ltd (China). (Z)-1-Methyl-3-((2*E*,4*E*)-5-(1-methyl-2-phenylindolizin-3-yl)- penta-2,4-dien-1-ylidene)-2-phenyl-3H-indolizin-4-ium Perchlorate (Dye 1 or **C5**) was prepared as previously described[24]. (*Z*)-7-(4-(dimethylamino)phenyl)-3-((2*E*,4*E*)-5-(7-(4-(dimethylamino)phenyl)-1-(2-ethylhexyl)-2-phenylindolizin-3-yl)penta-2,4-dien-1-ylidene)-1-(2-ethylhexyl)-2-phenyl-3*H*-indolizin-4-ium perchlorate (Dye 2 or **7-NMe2PhC5**) and (*Z*)-1-(2-ethylhexyl)-3-((2*E*,4*E*)-5-(1-(2-ethylhexyl)-2-phenylindolizin-3-yl)penta-2,4-dien-1-ylidene)-2-phenyl-3*H*-indolizin-4-ium perchlorate (Dye 3 or **1-EtHxC5**) were synthesized by Delcamp group.

### *2.2 Fabrication of PSCs*

Firstly, patterned ITO coated glass substrates were cleaned sequentially by detergent, acetone, deionized water, and isopropanol for 15 min in an ultrasonic bath. After that, the ITO substrates were dried by $N_2$ and treated with UV-ozone for 30 min. Then, the PTAA solution (3 mg/mL in chlorobenzene) was spin-coated on ITO glass at 4000 rpm for 30 s and the substrates were annealed at 100 ℃ for 10 min to form ITO/PTAA. The perovskite layer is prepared by a two-

step method. The perovskite precursor solution was prepared with 1.2 M $PbI_2$ and 0.3 M MAI in DMF:DMSO (10:1) mixed solvent. For preparation of the ITO/PTAA/$MAPbI_3$ thin film, the perovskite precursor solution was spin-coated on ITO/PTAA at 6000 rpm for 20 s and then MAI solution (30 mg/mL in IPA) was spin-coated at 4000 rpm for 40 s, then the substrates were annealed at 100 ℃ for 30 min. $PC_{61}BM$ (20 mg/mL in chlorobenzene) was spin-coated on the top of $MAPbI_3$ at 3000 rpm for 30 s. Then the ITO/PTAA/$MAPbI_3$/$PC_{61}BM$ substrates were annealed at 90 ℃ for 30 min. Afterwards, dye solutions in IPA with different concentrations were spin-coated on the top of $PC_{61}BM$ thin film at 4000 rpm for 30 s to form ITO/PTAA/$MAPbI_3$/$PC_{61}BM$/dye. Finally, the Ag electrode was fabricated by thermal evaporation under a vacuum of $6 \times 10^{-4}$ Pa. The active area for each cell is 0.04 $cm^2$ which is defined by a shadow mask.

*2.3 Film characterization*

The scanning electron microscopy (SEM) images were obtained by using a field emission scanning electron microscope (LYR3 XMH, Tescan). The material phase and crystallinity were studied by MiniFlex600 (Rigaku) with Cu Kα radiation source λ=1.54056 Å. The UV-vis absorption spectra of the films were collected by Cary 60 UV-vis spectrophotometer (Agilent Technologies). The current density with voltage and steady states of PSCs curves were measured by source meter (Keithley, 2400, USA) under the illumination AM1.5G (100mW/$cm^2$) of a G2V Pico solar simulator. The steady-state PL spectra were measured by a fluorescence spectrometer (FluoroMax, Horiba). The time-resolved photoluminescence (TRPL) spectra of devices were characterized by a time-correlated single-photon counting system (FluoroMax, Horiba) with DeltaHub and NanoLED. The electrochemical impedance spectra (EIS) were collected by an electrochemical workstation (CHI 604E) with a 0.9 V DC bias. The monochromatic incident photon-to-electron conversion efficiency (IPCE) spectra of devices were measured by a quantum efficiency measurement system (IQE-200B, Newport). The dark J-V curves of electron-only devices were collected from the source meter (Keithley, 2450, USA).

## 3. RESULTS AND DISCUSSIONS

The p-i-n PSCs are fabricated with the schematic structure of indium tin oxide (ITO)/PTAA/perovskite/$PC_{61}BM$/dye (with different molecule structures)/Ag (Figure 1a). The molecular structure of the dyes is displayed in the inset of Figure 1a. Figure 1b exhibits the energy

level alignment of the materials in our PSCs. The LUMO and HOMO states of the three dyes are obtained from the cyclic voltammogram data (Figure S1). PTAA and $PC_{61}BM$ are used as hole and electron transport layers, respectively. The electrons are transferred from $MAPbI_3$ to $PC_{61}BM$, then to the dye molecules. Finally, the electrons are collected by the Ag electrode. The holes are transported to ITO through the PTAA layer. The LUMOs of Dye1 and Dye3 locates at -4.25 eV and -4.22 eV, respectively, which are very similar to the work function of Ag (-4.2 eV)[24]. The LUMO of Dye2 locates at -4.10 eV, which have the best energy level matching between $PC_{61}BM$ and Ag. Therefore, it is expected that the electrons transport from $PC_{61}BM$ to Dye2 smoothly compared to Dye1 and Dye 3. Figure 1c and d show the SEM image of the $MAPbI_3$ film and cross-sectional SEM image of the device, respectively. $MAPbI_3$ grains with sizes of 250-500 nm are distributed densely to form the flat film (Figure 1c). The thicknesses of ITO/PTAA and perovskite layers are ~220, and ~250 nm, respectively. X-ray diffraction (XRD) patterns suggest that the crystal structure and crystallinity of $MAPbI_3$ films are not influenced by the dye modification (Figure 1e). Three XRD diffraction peaks at 14.25°, 28.60 °, and 32.05°are indexed to (110), (220), and (310) crystal planes of the perovskite, respectively. Figure 1f shows the absorption properties of perovskite film, $PC_{61}BM$/perovskite film, and perovskite/PC61BM films with the three dyes. The absorption peaks of the three perovskite/$PC_{61}BM$/dye films are located at ~750 nm, which is attributed to the absorption of the perovskite films. This illustrates three different dyes do not affect the 3D crystal structure of $MAPbI_3$ films.

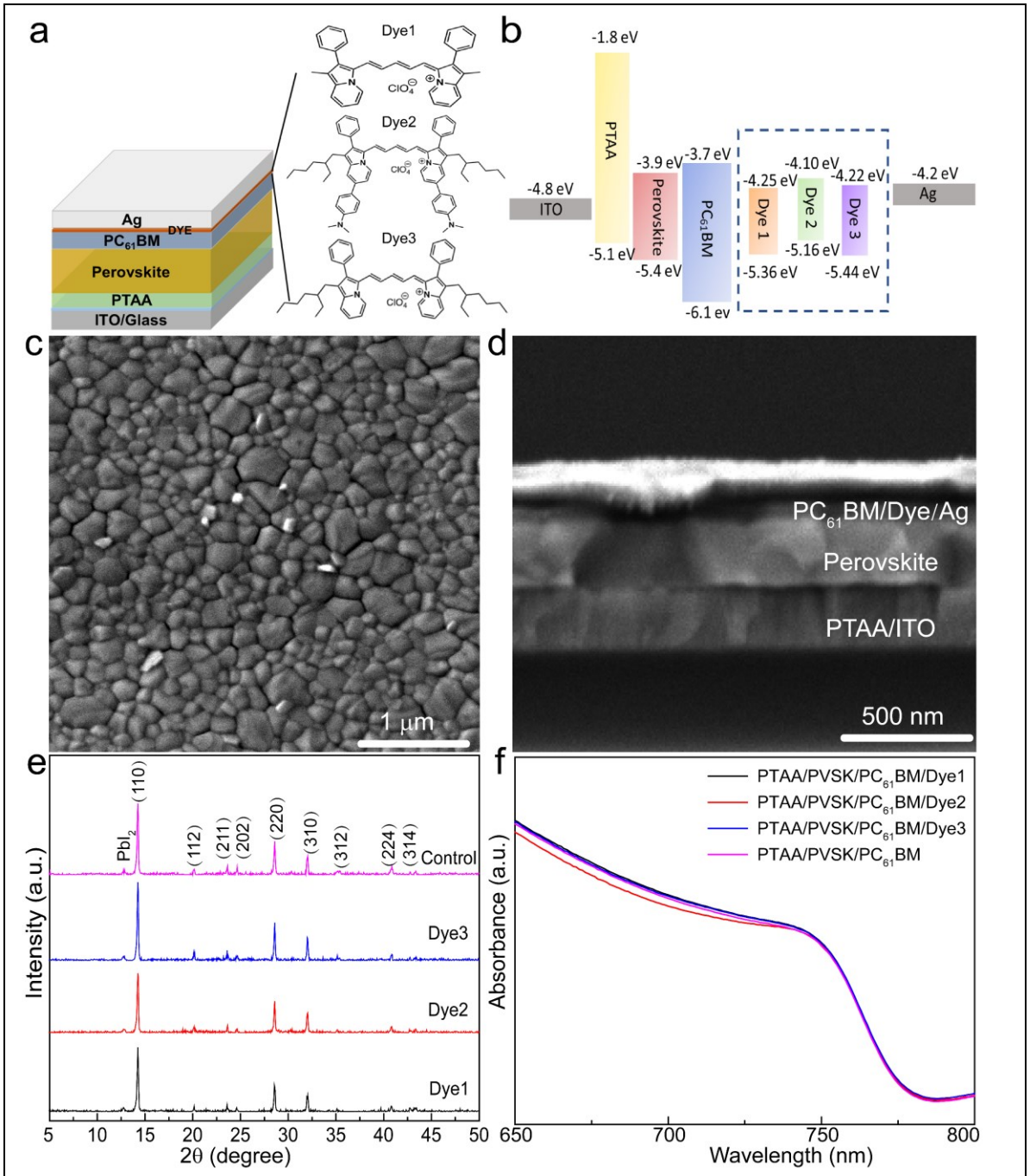


**Figure 1.** a) Structure of perovskite solar cell devices; b) Energy level alignment of the materials in PSCs; c) Top-view SEM image of the $MAPbI_3$ film; d) Cross-sectional SEM image of the device; e) XRD diffraction patterns of the $MAPbI_3$ films; f) The UV-vis spectra of PTAA/PVSK/$PC_{61}BM$, PTAA/PVSK/$PC_{61}BM$/Dye1, PTAA/PVSK/$PC_{61}BM$/Dye2 and PTAA/PVSK/$PC_{61}BM$/Dye3 films. PVSK=perovskite

AFM measurements are carried out to study the morphology and flatness of perovskite films affected by the interlayer dye molecules (Figure 2). Figure 2a, b, c, and d show the AFM images of ITO/PTAA/perovskite/$PC_{61}BM$/Dye1, ITO/PTAA/perovskite/$PC_{61}BM$/Dye2, ITO/PTAA/perovskite/$PC_{61}BM$/Dye3, and ITO/PTAA/perovskite/$PC_{61}BM$ films, respectively. It can be seen some small particles ~ 50 nm are observed to be distributed into the grain boundaries (GB) of the film from AFM figure, which modifies the GB and surface defects, leading to improved device performance. The small particles are attributed to the dye molecules. It is reported that the layering of dye molecules on $PC_{61}BM$ films prevents metal electrode migration[25], leading to excellent device performance. Moreover, the root mean square (RMS) values of the perovskite film with Dye1, Dye2, and Dye3 are 2.94, 4.93 and 3.63 nm, respectively. While the bare film

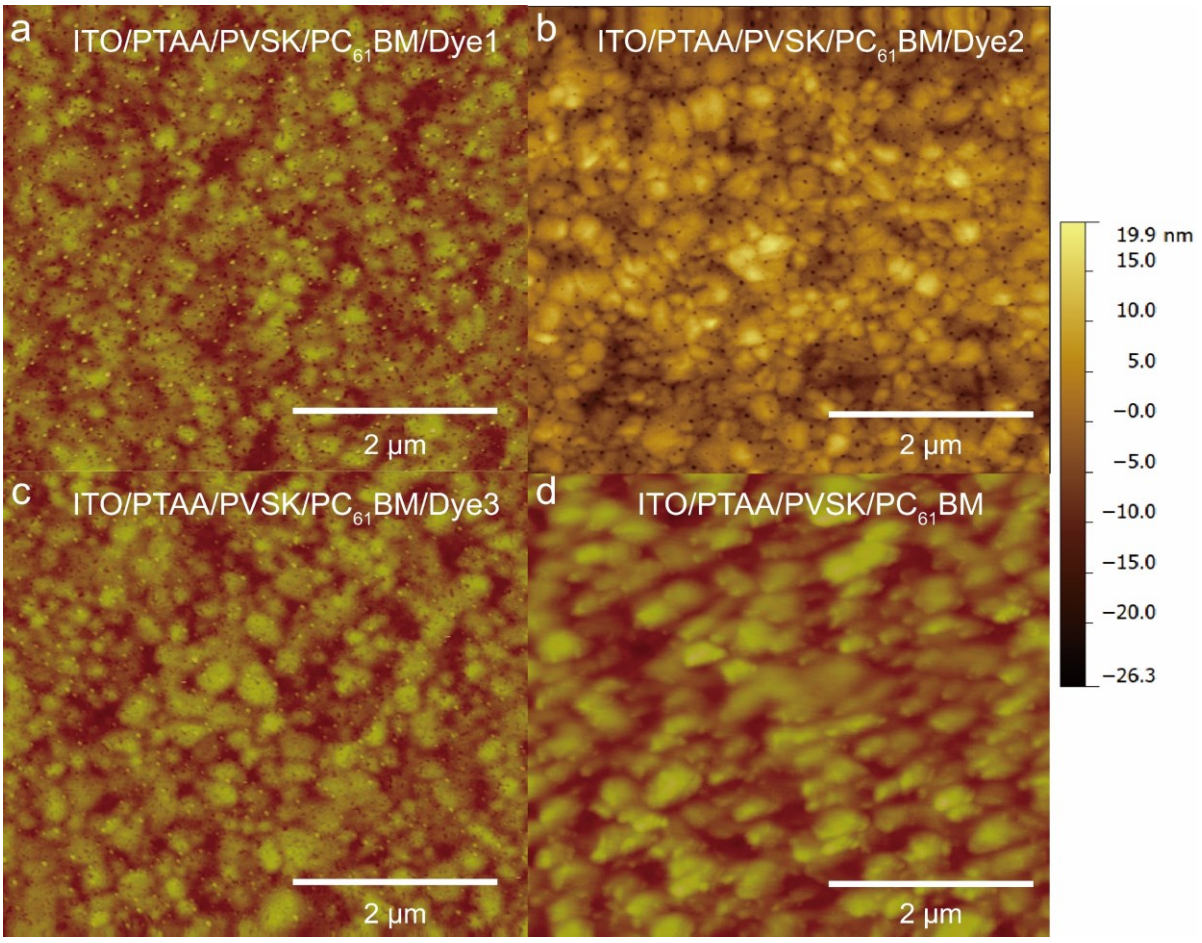


**Figure 2.** a) AFM image of PTAA/PVSK/$PC_{61}BM$/Dye1 film, b) AFM image of PTAA/PVSK/$PC_{61}BM$/Dye2 film, c) AFM image of PTAA/PVSK/$PC_{61}BM$/Dye3 film and d) AFM image of PTAA/PVSK/$PC_{61}BM$ film. PVSK=perovskite

presents an RMS value of 7.69 nm. Therefore, the perovskite films with dye molecules are more uniform and smoother compared to the bare film. The interlayer passivation by the dye molecules between $PC_{61}BM$ and Ag exhibits significant potential in eliminating interface defects to allow for the fabrication of high-performance devices. Modification of perovskite films with Dye1 shows better interface contact than that of Dye2 and Dye3, which is attributed to the short chains of Dye1.

PSCs with different dye concentrations are fabricated to study the influence of dye passivation on device performance, and the results are shown in Figure 3. Figure 3 a-c show the (power conversion efficiency) PCE distribution of PSCs with Dye1, Dye2, and Dye3 as well as the bare PSCs. The performance of PSCs increases as the dye concentrations increase from 0.25 mg/mL to 0.75 mg/mL, then decrease as the dye concentrations further increase to 1.0 mg/mL for all three dyes. So, the optimal concentrations of all three dyes are 0.75 mg/mL (in IPA). The statistical photovoltaic parameter values including short-circuit current density (Jsc), open-circuit voltage (Voc), and fill factor (FF) of the PSCs based on different dye concentrations are shown in Figure S2. The FF values of control devices are obtained based on eight devices fabricated with the same experimental parameters. The highest FF for our control devices is ~65%, which is

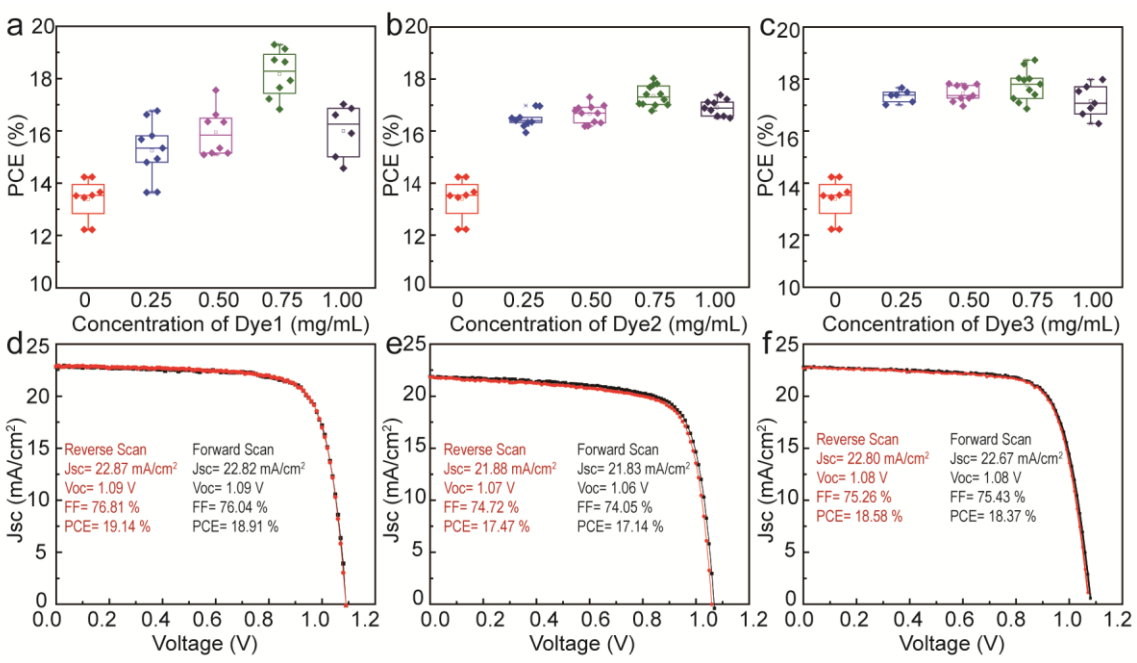


**Figure 3.** a-c) The PCE distributions of PSCs with different concentrations of Dye1, Dye2 and Dye3; d-f) The best devices with Dye1, Dye2 and Dye3.

similar to the results of Zhang *et al.* (FF=60.29%), John Ciro *et al.* (FF=66.68%), Lu-Lu Jiang *et*

*al.* (FF=59%), Wei Chen *et al.* (FF=60%) and Zhiqiang Zhao *et al.* (FF=68.07%) for the same device structure[26–29]. Figure 3 d-f display the best devices with the three dyes in this work. The PSC with Dye1 exhibits a PCE of 19.14% with a Jsc of 22.87mA/cm$^2$, a Voc of 1.09 V, and an FF of 76.81%. The PSC with Dye2 shows a PCE of 17.47% with a Jsc of 21.88 mA/cm$^2$, a Voc of 1.07 V, and an FF of 74.72%.

The PSC with the Dye3 modification represents a PCE of 18.58% with a Jsc of 22.80 mA/cm$^2$, a Voc of 1.08 V, and an FF of 75.26 %. The PSC with Dye1 exhibits higher performance than the PSCs with Dye2 and Dye3. This is attributed to an optimized interface contact between Dye1 and $PC_{61}BM$ when compared to that of Dye2 and Dye3 (Figure 2). Therefore, electrons are transferred from $PC_{61}BM$ to Dye1 much easier than Dye2 and Dye3. In addition, the hysteresis index values ($HI=(PCE_{reverse}-PCE_{forward})/PCE_{reverse}$) of PSCs with Dye1, Dye2, and Dye3 are calculated to be 0.012, 0.019, and 0.011, respectively, which are much smaller than the control device (0.040). $PCE_{reverse}$ and $PCE_{forward}$ are the PCE values obtained under reverse and forward scan directions, respectively. This is explained by reduced charge recombination due to interface passivation by the dye molecules [16,30–32]. The integrated current values are 19.3, 18.9, 19.0 and 18.7 mA/cm$^2$ for Dye1, Dye2, Dye3 and control, respectively, which are shown in Table 1. The integrated current is mismatched with the Jsc from J-V curves. The difference values between the cell current and the integral current are 12.5%, 15.6%, 13.6%, and 16.6% for control, Dye1, Dye2, and Dye3 devices. Recently, Etgar *et. al.* claimed that the Jsc measured from J-V curves is accurate when the integrated current is less than Jsc within 10-20 %. The measuring light of the IPCE and J-V curves are different. The typical IPCE setup uses Xe lamp with a monochromator as the light source. J-V curves are obtained from a solar simulator with 1 sun illumination. In addition, the ion migration and degradation of the perovskite films during a relatively long measurement time result in lower Jsc values obtained from IPCE measurements. The ion movement inside the perovskite films caused by the external bias is another reason for the decreased Jsc for the IPCE measurements. The last reason is the frequency dependence of the IPCE measurement. Therefore, 10-20 % difference should be accepted[33].

In order to study the mechanisms of the improved device performance by dye molecules, optical, electrochemical, and photoelectrical properties of the devices are investigated. Figure 4a shows the IPCE spectra of PSCs with the dyes. All devices have an IPCE response in the 300-800

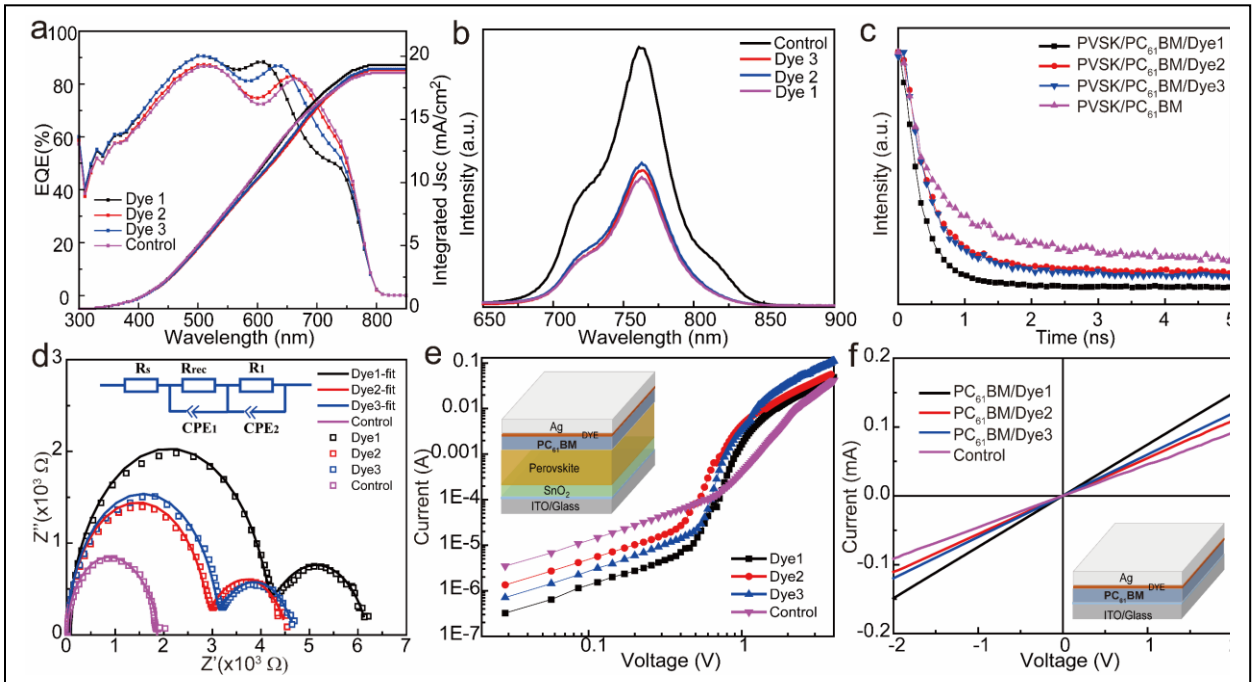


**Figure 4.** a) The IPCE spectra and integrated current curves of PSCs with and without dyes; b) The PL spectra of PVSK/$PC_{61}BM$, PVSK/$PC_{61}BM$/Dye1, PVSK/$PC_{61}BM$/Dye2, PVSK/$PC_{61}BM$/Dye3 films; c) TRPL spectra of PSCs with the three dyes and. a control sample; d) Nyquist plots of the PSCs with and without dyes under 0.9 V; e) J-V curves of the electron electron-only devices with the three dyes; f) J-V curves of the Ag electrodes with and without the three dyes. PVSK=perovskite

nm range, which is consistent with the UV-vis absorption spectra shown in Figure 1f. The additional dye interface passivation layer significantly improves the photoresponse of the devices in all the working wavelengths. The peaks in the region of 600-700 nm in the IPCE spectra of devices exhibit blueshift. This is attributed to the redistribution of the optical electric field of devices by the interface layers[34,35]. Figure 4b and c show the steady-state photoluminescence (PL) and time-resolved photoluminescence (TRPL) spectra of perovskite/$PC_{61}BM$/dye films, respectively. It can be seen from Figure 4b that the steady-state PL spectra of the perovskite/$PC_{61}BM$/dye films show decreased intensities compared to the perovskite/$PC_{61}BM$ film, indicating that the dye interface passivation facilitates charge transport between $PC_{61}BM$ and the Ag electrode. For the TRPL spectra of films (perovskite/$PC_{61}BM$, perovskite/$PC_{61}BM$/dye), the lifetime is fitted with a bi-exponential function (equation 1).

$$Y = A_1 \exp\left(\frac{-t}{\tau_1}\right) + A_2 \exp\left(\frac{-t}{\tau_2}\right) \quad (1)$$

where $A_1$ and $A_2$ are the relative amplitudes; t means time; $\tau_1$ and $\tau_2$ are the lifetime values for the fast and slow decay, respectively. The detailed fitting parameters are shown in Table 1. The charge recombination caused by defects influences the fast decay ($\tau_1$), and the radiative recombination affects the slow decay ($\tau_2$)[7,36]. The lifetime of bare perovskite film is ~ 311 ns ($\tau_1$=14 ns, $\tau_2$=440 ns). The lifetime of perovskite/$PC_{61}BM$ film is 11.53 ns ($\tau_1$=30.32 ns and $\tau_2$=9.14 ns). The lifetime values of perovskite/$PC_{61}BM$/Dye1, perovskite/$PC_{61}BM$/Dye2, and perovskite/$PC_{61}BM$/Dye3 films are 4.09 ns, ($\tau_1$=10.84 ns $\tau_2$=2.78 ns), 9.55 ns ($\tau_1$=33.92 ns and $\tau_2$ =3.78 ns), and 7.79 ns ($\tau_1$=49.82 ns and $\tau_2$=2.76 ns), respectively. The shorter lifetime of perovskite/$PC_{61}BM$/dye compared to perovskite/$PC_{61}BM$ indicates improved charge extraction. In addition, the devices with Dye1 as interface layer have better charge transport to $PC_{61}BM$ than Dye2 and Dye3caused by the film roughness which is consistent with Figure 2. The TRPL results are consistent with the PL results. Therefore, the dye interface passivation layer enhances the charge transfer from the perovskite film to the Ag electrode.

To further evaluate the influence of the dyes on charge recombination in PSCs, the electrical impedance spectroscopy (EIS) data of the devices are measured at a bias of 0.9 V under dark (Figure 4d). The equivalent circuit is shown in the inset of Figure 4d, where $R_s$ is attributed to series resistance (wire and ITO); $R_{rec}$ is related to the recombination resistance of the devices; $CPE_1$ is the contact capacitance; $R_1$ is the dielectric relaxation resistance; $CPE_2$ is the capacitance of perovskite films. There are two semicircle characteristics of all devices in the Nyquist plots, wherein the high-frequency component is related to the charge recombination processes, and the low-frequency component is associated with the dielectric relaxation[37]. $R_{rec}$ values of the devices with Dye1, Dye2, and Dye3 are 4091 Ω, 2853 Ω, and 3053 Ω, respectively, which are much higher than the control device (1753 Ω). This means the dye interface passivation layers suppress charge recombination at the interface of $PC_{61}BM$ and Ag. Dye1 shows better performance than the other dyes, which may be attributed to the optimized interface contact (Figure 2). The influence of the dye interface passivation layer on the charge mobility and non-radiative recombination loss of PSCs is studied by the dark J-V curves of the electrons-only devices (Figure 4e), and the structure of the devices is shown in the inset of Figure 4e (ITO/$SnO_2$/$MAPbI_3$/$PC_{61}BM$/dye/Ag).

**Table 1.** Summary of photovoltaic parameters and EIS parameters of the PSCs with and without the three dyes under 0.9 V.

| Sample | Jsc (mA/cm$^2$) | integrated Jsc (mA/cm$^2$) | Voc (V) | FF (%) | PCE (%) | $R_s$ (Ω) | $R_{rec}$ (Ω) |
|---|---|---|---|---|---|---|---|
| Dye1 | 22.87 | 19.3 | 1.09 | 76.81 | 19.14 | 21.96 | 4091 |
| Dye2 | 21.88 | 18.9 | 1.07 | 74.72 | 17.47 | 19.99 | 2853 |
| Dye3 | 22.80 | 19.0 | 1.08 | 75.26 | 18.58 | 22.67 | 3053 |
| Control | 21.37 | 18.7 | 1.04 | 64.26 | 14.24 | 18.08 | 1753 |

The J-V curves show three different regions ($J \propto V^n$) including: the ohmic behavior (n=1), the trap-filled limit (TFL) region (n>3), and the space-charge limited current (SCLC) region (n=2)[38]. The charge mobility (μ) is calculated by equation (2) in the SCLC region[39].

$$J_d = \frac{9}{8}\varepsilon\varepsilon_0\mu\frac{V^2}{L^3} \quad (2)$$

where $J_d$ is the dark injection current, V is the bias voltage, $\varepsilon_0$ and ε are the vacuum dielectric constant and the relative dielectric constant of $MAPbI_3$, respectively, and L is the thickness of perovskite film (≈250 nm). The electron mobilities of devices with Dye1, Dye2, and Dye3 are $4.90\times10^{-2}$ cm$^2$/Vs, $3.86\times10^{-2}$ cm$^2$/Vs, and $4.83\times10^{-2}$ cm$^2$/Vs respectively, which are much larger than the control device ($2.17\times10^{-2}$ cm$^2$/Vs). The mobility measurements suggest the dye interface passivation layers help charge transportation and reduce the recombination loss at the interface of $PC_{61}BM$ and Ag. The trap density of devices ($n_t$) is calculated by equation (3)[17,40].

$$V_{TFL} = \frac{en_tL^2}{2\varepsilon\varepsilon_0} \quad (3)$$

Where e is the elementary charge of electrons, L is the thickness of the perovskite film, ε is the relative dielectric constant of $MAPbI_3$, $\varepsilon_0$ is the vacuum dielectric constant, $V_{TFL}$ is the onset voltage of TFL. The calculated electron trap density values of the devices based on Dye1, Dye2, and Dye3 are $2.72\times10^{18}$ cm$^{-3}$, $2.91\times10^{18}$ cm$^{-3,}$ and $2.86\times10^{18}$ cm$^{-3}$, which are smaller than the control device ($4.41\times10^{18}$ cm$^{-3}$). The electron trap density of devices decreases by introducing the dye interface passivation layers, leading to improved devices performance. J–V characteristics of devices with the configuration of ITO/$PC_{61}BM$/dye/Ag are shown in Figure 4f.

The device structure is exhibited in the insert of Figure 4f. The slope of the curves in the Figure 4f is the resistivity of the devices according to the literature[17]. The conductivity (σ) can be calculated by equation (4)[41].

$$I = \frac{\sigma SV}{d} \quad (4)$$

where S is the device area, and d is the thickness of the film. The conductivity values of the devices with Dye1, Dye2, and Dye3 are $8.41\times10^{-3}$, $1.13\times10^{-2}$, and $1.04\times10^{-2}$ S/m, respectively. The control device shows a conductivity of $1.37\times10^{-2}$ S/m. The device with the low slope has a large contact resistance and a large charge injection barrier. The devices with the structure of ITO/$PC_{61}BM$/dye/Ag have larger slopes than that of the ITO/$PC_{61}BM$/Ag. So, the contact resistance is reduced by the dye interface passivation layer, leading to effective charge transport. The contact resistance of the device based on Dye1 is smaller than that of Dye2 and Dye3, which is consistent with the J-V and EIS results. PL spectra, TRPL spectra, EIS spectra, and electron-only devices all confirm that the dye interface passivation layer reduces charge recombination at the interface of $PC_{61}BM$ and Ag, leading to improved PSC device performance. Dye1 modification leads to better interface contact than that of Dye2 and Dye3 (Figure 2). However, Dye1 and Dye3 have near identical energy level. Therefore, the interface contact is a dominant factor with respect to device performances. In addition, the chain length also influences the charge transport among the layers. It is reported that the longer chain at the interfaces is associated with the large tunneling barrier for charge transport through the chains. Dye1 shows the shortest chain in the three dyes (Figure 1). Dye 3 shows a shorter chain than Dye2. Therefore, short chains can modify the interface better in our work[42–44].

The influence of the dye interface passivation layer on the stability of PSCs is also studied. Figure 5a shows the stability of PSCs under continuous light illumination. The control and modified devices are measured at the maximum power point. The modified and control devices exhibit slowly decay and show stable PCE for 350 s. The air stability of devices is shown in Figure 5b. The devices with Dye1, Dye2, and Dye3 remain about 90%, 60%, and 80% of the initial PCE after 120 h exposure in the air (25℃ and 30±5 % RH), respectively. The control device only retains 49% of the initial PCE under the same conditions. The enhanced air stability of the devices

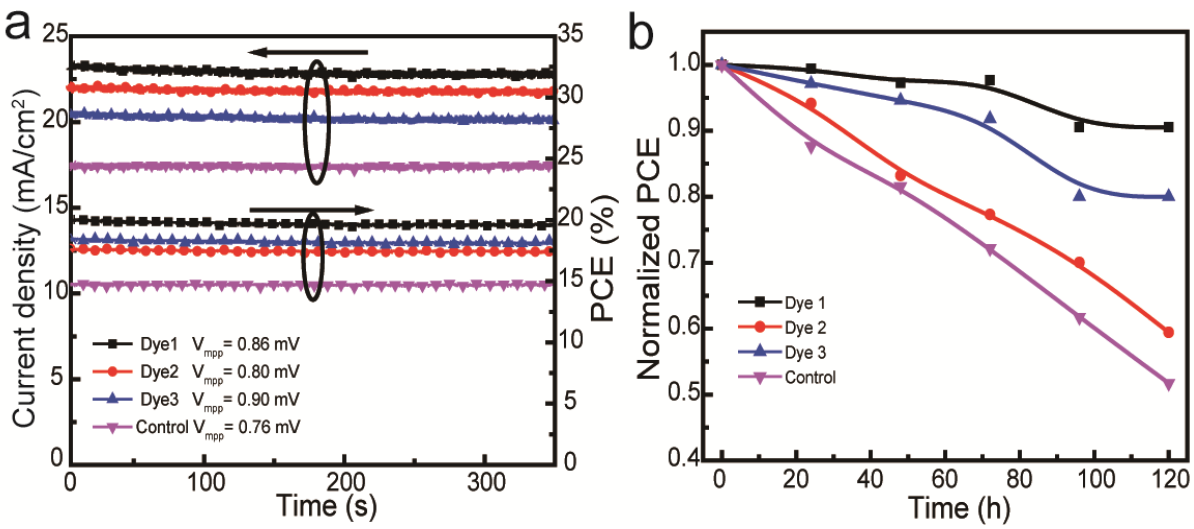


**Figure 5.** a) Light stability of PSCs devices with and without the three dyes; b) The time stability of PSCs devices with and without the three dyes.

modified with dye can be explained by the reduced ion migration caused by reduced interfacial charge recommendation.

## 4. CONCLUSIONS

Three dye molecules are used as an interfacial passivation layer at the interface between $PC_{61}BM$ and Ag electrode in the inverse PSCs to improve the device performance. The Dye1, Dye2, and Dye3 interface passivation layer reduces the energy barrier between $PC_{61}BM$ and Ag. All the dyes suppress the charge recombination at the interfaces in the devices. Moreover, the dye interface passivation layer enhances the charge transport and decreases the trap state density of the $PC_{61}BM$ film. The PCE of PSC devices with Dye1, Dye2, and Dye3 increase from a control value of 14.24% to 19.14%, 17.47%, and 18.58%, respectively. Interface contact appears to be a

dominant factor since the three dyes with near identical energy levels and identical conjugated systems have significantly different performances. In addition, PSCs with the dyes exhibit better stability than the control devices. The interface passivation layer also likely protects the PSCs from moisture. PSC devices with Dye1 maintain about 90% of the initial PCE under ambient environment (25℃ and 30±5 % RH) for 120 h.

ASSOCIATED CONTENT

**Supporting Information**

Cyclic voltammograms of three dyes and the Jsc, Voc and FF distributions of perovskite solar cells with different concentrations of three dyes.

Author Information

*Corresponding Author*

**Qilin Dai**: *Department of Chemistry, Physics, and Atmospheric Sciences, Jackson State University, Jackson, Mississippi, 39217, United States.*

Email: *qilin.dai@jsums.edu*

*Authors*

**Yifang Qi**: *Department of Chemistry, Physics, and Atmospheric Sciences, Jackson State University, Jackson, Mississippi, 39217, United States*

**William E. Meador**: *Department of Chemistry and Biochemistry, University of Mississippi, Oxford, Mississippi 38677, United States*

**Jared Delcamp**: *Department of Chemistry and Biochemistry, University of Mississippi, Oxford, Mississippi 38677, United States*

**Ndaleh David**: *Department of Chemistry and Biochemistry, University of Mississippi, Oxford, Mississippi 38677, United States*

**Glake Hill**: *Department of Chemistry, Physics, and Atmospheric Sciences, Jackson State University, Jackson, Mississippi, 39217, United States*

**Nihar Pradhan**: *Department of Chemistry, Physics, and Atmospheric Sciences, Jackson State University, Jackson, Mississippi, 39217, United States*

*Author Contributions*

Yifang Qi carried out the experiments and wrote the draft of the manuscript. Ndaleh David, William E. Meador, and Jared Delcamp synthesized the NIR dyes. Glake Hill helped with the understanding of the passivation. Nihar Pradhan did AFM measurement. Qilin Dai supervised the project. All authors have approved the final version of the manuscript.

*Notes*

The authors declare no competing financial interest.

ACKNOWLEDGMENT

This material is based on work supported by the National Science Foundation under Grant No. 1757220. The steady-state PL and TRPL equipment used in this work is supported by National Science Foundation Research Initiation Award: Novel Perovskite Solar Cells Based on Interface Manipulation (Award#1900047).

REFERENCES

(1) Best Research-Cell Efficiency Chart https://www.nrel.gov/pv/cell-efficiency.html (accessed 2021 -06 -05).

(2) Yang, Y.; Wu, J.; Wang, X.; Guo, Q.; Liu, X.; Sun, W.; Wei, Y.; Huang, Y.; Lan, Z.; Huang, M.; Lin, J.; Chen, H.; Wei, Z. Suppressing Vacancy Defects and Grain Boundaries via Ostwald Ripening for High-Performance and Stable Perovskite Solar Cells. *Adv. Mater.* **2020**, *32* (7), 1904347.

(3) Wang, S.; Li, Z.; Zhang, Y.; Liu, X.; Han, J.; Li, X.; Liu, Z.; Liu, S. (Frank); Choy, W. C. H. Water-Soluble Triazolium Ionic-Liquid-Induced Surface Self-Assembly to Enhance the Stability and Efficiency of Perovskite Solar Cells. *Adv. Funct. Mater.* **2019**, *29* (15), 1900417.

(4) Liu, K.; Liang, Q.; Qin, M.; Shen, D.; Yin, H.; Ren, Z.; Zhang, Y.; Zhang, H.; Fong, P. W. K.; Wu, Z.; Huang, J.; Hao, J.; Zheng, Z.; So, S. K.; Lee, C.-S.; Lu, X.; Li, G. Zwitterionic-Surfactant-Assisted Room-Temperature Coating of Efficient Perovskite Solar Cells. *Joule* **2020**, *4* (11), 2404–2425.

(5) Yang, G.; Chen, C.; Yao, F.; Chen, Z.; Zhang, Q.; Zheng, X.; Ma, J.; Lei, H.; Qin, P.; Xiong, L.; Ke, W.; Li, G.; Yan, Y.; Fang, G. Effective Carrier-Concentration Tuning of $SnO_2$ Quantum Dot Electron-Selective Layers for High-Performance Planar Perovskite Solar Cells. *Adv. Mater.* **2018**, *30* (14), 1706023.

(6) Wu, Y.; Xie, F.; Chen, H.; Yang, X.; Su, H.; Cai, M.; Zhou, Z.; Noda, T.; Han, L. Thermally Stable $MAPbI_3$ Perovskite Solar Cells with Efficiency of 19.19% and Area over 1 $Cm^2$ Achieved by Additive Engineering. *Adv. Mater.* **2017**, *29* (28), 1701073.
(7) Jiang, Q.; Zhao, Y.; Zhang, X.; Yang, X.; Chen, Y.; Chu, Z.; Ye, Q.; Li, X.; Yin, Z.; You, J. Surface Passivation of Perovskite Film for Efficient Solar Cells. *Nat. Photonics* **2019**, *13* (7), 460–466.
(8) J. Yoo, J.; Wieghold, S.; C. Sponseller, M.; R. Chua, M.; N. Bertram, S.; Putri Hartono, N. T.; S. Tresback, J.; C. Hansen, E.; Correa-Baena, J.-P.; Bulović, V.; Buonassisi, T.; Sik Shin, S.; G. Bawendi, M. An Interface Stabilized Perovskite Solar Cell with High Stabilized Efficiency and Low Voltage Loss. *Energy Environ. Sci.* **2019**, *12* (7), 2192–2199.
(9) Kim, M.; Kim, G.-H.; Lee, T. K.; Choi, I. W.; Choi, H. W.; Jo, Y.; Yoon, Y. J.; Kim, J. W.; Lee, J.; Huh, D.; Lee, H.; Kwak, S. K.; Kim, J. Y.; Kim, D. S. Methylammonium Chloride Induces Intermediate Phase Stabilization for Efficient Perovskite Solar Cells. *Joule* **2019**, *3* (9), 2179–2192.
(10) Wu, S.; Zhang, J.; Li, Z.; Liu, D.; Qin, M.; Cheung, S. H.; Lu, X.; Lei, D.; So, S. K.; Zhu, Z.; Jen, Alex. K.-Y. Modulation of Defects and Interfaces through Alkylammonium Interlayer for Efficient Inverted Perovskite Solar Cells. *Joule* **2020**, *4* (6), 1248–1262.
(11) Li, N.; Tao, S.; Chen, Y.; Niu, X.; Onwudinanti, C. K.; Hu, C.; Qiu, Z.; Xu, Z.; Zheng, G.; Wang, L.; Zhang, Y.; Li, L.; Liu, H.; Lun, Y.; Hong, J.; Wang, X.; Liu, Y.; Xie, H.; Gao, Y.; Bai, Y.; Yang, S.; Brocks, G.; Chen, Q.; Zhou, H. Cation and Anion Immobilization through Chemical Bonding Enhancement with Fluorides for Stable Halide Perovskite Solar Cells. *Nat. Energy* **2019**, *4* (5), 408–415.
(12) Jung, E. H.; Jeon, N. J.; Park, E. Y.; Moon, C. S.; Shin, T. J.; Yang, T.-Y.; Noh, J. H.; Seo, J. Efficient, Stable and Scalable Perovskite Solar Cells Using Poly(3-Hexylthiophene). *Nature* **2019**, *567* (7749), 511–515.
(13) Kim, Y. Y.; Yang, T.-Y.; Suhonen, R.; Kemppainen, A.; Hwang, K.; Jeon, N. J.; Seo, J. Roll-to-Roll Gravure-Printed Flexible Perovskite Solar Cells Using Eco-Friendly Antisolvent Bathing with Wide Processing Window. *Nat. Commun.* **2020**, *11* (1), 5146.
(14) Song, S.; Kang, G.; Pyeon, L.; Lim, C.; Lee, G.-Y.; Park, T.; Choi, J. Systematically Optimized Bilayered Electron Transport Layer for Highly Efficient Planar Perovskite Solar Cells ($\eta = 21.1\%$). *ACS Energy Lett.* **2017**, *2* (12), 2667–2673.
(15) Wolff, C. M.; Zu, F.; Paulke, A.; Toro, L. P.; Koch, N.; Neher, D. Reduced Interface-Mediated Recombination for High Open-Circuit Voltages in $CH_3NH_3PbI_3$ Solar Cells. *Adv. Mater.* **2017**, *29* (28), 1700159.
(16) Liu, Y.; Bag, M.; Renna, L. A.; Page, Z. A.; Kim, P.; Emrick, T.; Venkataraman, D.; Russell, T. P. Understanding Interface Engineering for High-Performance Fullerene/Perovskite Planar Heterojunction Solar Cells. *Adv. Energy Mater.* **2016**, *6* (2), 1501606.
(17) Xiong, S.; Yuan, M.; Yang, J.; Song, J.; Guo, X.; Li, X.; Li, B.; Liu, X.; Duan, C.; Liu, F.; Fahlman, M.; Bao, Q. Engineering of the Back Contact between PCBM and Metal Electrode for Planar Perovskite Solar Cells with Enhanced Efficiency and Stability. *Adv. Opt. Mater.* **2019**, *7* (19), 1900542.
(18) Guarnera, S.; Abate, A.; Zhang, W.; Foster, J. M.; Richardson, G.; Petrozza, A.; Snaith, H. J. Improving the Long-Term Stability of Perovskite Solar Cells with a Porous $Al_2O_3$ Buffer Layer. *J. Phys. Chem. Lett.* **2015**, *6* (3), 432–437.
(19) Li, M.; Zhao, C.; Wang, Z.-K.; Zhang, C.-C.; Lee, H. K. H.; Pockett, A.; Barbé, J.; Tsoi, W. C.; Yang, Y.-G.; Carnie, M. J.; Gao, X.-Y.; Yang, W.-X.; Durrant, J. R.; Liao, L.-S.; Jain,

S. M. Interface Modification by Ionic Liquid: A Promising Candidate for Indoor Light Harvesting and Stability Improvement of Planar Perovskite Solar Cells. *Adv. Energy Mater.* **2018**, *8* (24), 1801509.

(20) Zhang, H.; Azimi, H.; Hou, Y.; Ameri, T.; Przybilla, T.; Spiecker, E.; Kraft, M.; Scherf, U.; Brabec, C. J. Improved High-Efficiency Perovskite Planar Heterojunction Solar Cells via Incorporation of a Polyelectrolyte Interlayer. *Chem. Mater.* **2014**, *26* (18), 5190–5193.

(21) Deng, Y.; Peng, E.; Shao, Y.; Xiao, Z.; Dong, Q.; Huang, J. Scalable Fabrication of Efficient Organolead Trihalide Perovskite Solar Cells with Doctor-Bladed Active Layers. *Energy Environ. Sci.* **2015**, *8* (5), 1544–1550.

(22) Jeng, J.-Y.; Chiang, Y.-F.; Lee, M.-H.; Peng, S.-R.; Guo, T.-F.; Chen, P.; Wen, T.-C. $CH_3NH_3PbI_3$ Perovskite/Fullerene Planar-Heterojunction Hybrid Solar Cells. *Adv. Mater.* **2013**, *25* (27), 3727–3732.

(23) Xiao, P.; Alam Sk, M.; Thia, L.; Ge, X.; Jern Lim, R.; Wang, J.-Y.; Hwa Lim, K.; Wang, X. Molybdenum Phosphide as an Efficient Electrocatalyst for the Hydrogen Evolution Reaction. *Energy Environ. Sci.* **2014**, *7* (8), 2624–2629.

(24) Ye, S.; Sun, W.; Li, Y.; Yan, W.; Peng, H.; Bian, Z.; Liu, Z.; Huang, C. CuSCN-Based Inverted Planar Perovskite Solar Cell with an Average PCE of 15.6%. *Nano Lett.* **2015**, *15* (6), 3723–3728.

(25) Wang, Q.; Abate, A. Strategies toward Stable Perovskite Solar Cells. *Adv. Mater. Interfaces* **2018**, *5* (22), 1800264.

(26) Zhang, H.; Azimi, H.; Hou, Y.; Ameri, T.; Przybilla, T.; Spiecker, E.; Kraft, M.; Scherf, U.; Brabec, C. J. Improved High-Efficiency Perovskite Planar Heterojunction Solar Cells via Incorporation of a Polyelectrolyte Interlayer. *Chem. Mater.* **2014**, *26* (18), 5190–5193.

(27) Zhao, Z.; Huang, J.; Cao, Y.; Sun, Z.-Z.; Cheng, N.; Sun, S.; Sun, H.; You, S. Inverted Planar Perovskite Solar Cells with Efficient and Stability via Optimized Cathode-Interfacial Layer. *Sol. Energy* **2020**, *207*, 1165–1171.

(28) Ciro, J.; Mesa, S.; Uribe, J. I.; Mejía-Escobar, M. A.; Ramirez, D.; Montoya, J. F.; Betancur, R.; Yoo, H.-S.; Park, N.-G.; Jaramillo, F. Optimization of the Ag/PCBM Interface by a Rhodamine Interlayer to Enhance the Efficiency and Stability of Perovskite Solar Cells. *Nanoscale* **2017**, *9* (27), 9440–9446.

(29) Chen, W.; Zhu, Y.; Yu, Y.; Xu, L.; Zhang, G.; He, Z. Low Cost and Solution Processed Interfacial Layer Based on Poly(2-Ethyl-2-Oxazoline) Nanodots for Inverted Perovskite Solar Cells. *Chem. Mater.* **2016**, *28* (14), 4879–4883.

(30) Meng, X.; Ho, C. H. Y.; Xiao, S.; Bai, Y.; Zhang, T.; Hu, C.; Lin, H.; Yang, Y.; So, S. K.; Yang, S. Molecular Design Enabled Reduction of Interface Trap Density Affords Highly Efficient and Stable Perovskite Solar Cells with over 83% Fill Factor. *Nano Energy* **2018**, *52*, 300–306.

(31) Wang, C.; Liu, P.; Ju, H.; Yuan, Q.; Han, D.; Wang, Y.; Zhou, D.-Y.; Feng, L. A Simple Perylene Derivative as a Solution-Processable Cathode Interlayer for Perovskite Solar Cells with Enhanced Efficiency and Stability. *ACS Appl. Mater. Interfaces* **2018**, *10* (18), 15933–15942.

(32) Kang, D.-H.; Park, N.-G. On the Current–Voltage Hysteresis in Perovskite Solar Cells: Dependence on Perovskite Composition and Methods to Remove Hysteresis. *Adv. Mater.* **2019**, *31* (34), 1805214.

(33) Saliba, M.; Etgar, L. Current Density Mismatch in Perovskite Solar Cells. *ACS Energy Lett.* **2020**, *5* (9), 2886–2888.

(34) Gilot, J.; Barbu, I.; Wienk, M. M.; Janssen, R. A. J. The Use of ZnO as Optical Spacer in Polymer Solar Cells: Theoretical and Experimental Study. *Appl. Phys. Lett.* **2007**, *91* (11), 113520.
(35) Xiong, J.; Dai, Z.; Zhan, S.; Zhang, X.; Xue, X.; Liu, W.; Zhang, Z.; Huang, Y.; Dai, Q.; Zhang, J. Multifunctional Passivation Strategy Based on Tetraoctylammonium Bromide for Efficient Inverted Perovskite Solar Cells. *Nano Energy* **2021**, *84*, 105882.
(36) Yin, J.; Cao, J.; He, X.; Yuan, S.; Sun, S.; Li, J.; Zheng, N.; Lin, L. Improved Stability of Perovskite Solar Cells in Ambient Air by Controlling the Mesoporous Layer. *J. Mater. Chem. A* **2015**, *3* (32), 16860–16866.
(37) Li, J.; Wang, H.; Chin, X. Y.; Dewi, H. A.; Vergeer, K.; Goh, T. W.; Lim, J. W. M.; Lew, J. H.; Loh, K. P.; Soci, C.; Sum, T. C.; Bolink, H. J.; Mathews, N.; Mhaisalkar, S.; Bruno, A. Highly Efficient Thermally Co-Evaporated Perovskite Solar Cells and Mini-Modules. *Joule* **2020**, *4* (5), 1035–1053.
(38) Shi, D.; Adinolfi, V.; Comin, R.; Yuan, M.; Alarousu, E.; Buin, A.; Chen, Y.; Hoogland, S.; Rothenberger, A.; Katsiev, K.; Losovyj, Y.; Zhang, X.; Dowben, P. A.; Mohammed, O. F.; Sargent, E. H.; Bakr, O. M. Low Trap-State Density and Long Carrier Diffusion in Organolead Trihalide Perovskite Single Crystals. *Science* **2015**, *347* (6221), 519–522.
(39) Ma, J.; Zheng, M.; Chen, C.; Zhu, Z.; Zheng, X.; Chen, Z.; Guo, Y.; Liu, C.; Yan, Y.; Fang, G. Efficient and Stable Nonfullerene-Graded Heterojunction Inverted Perovskite Solar Cells with Inorganic $Ga_2O_3$ Tunneling Protective Nanolayer. *Adv. Funct. Mater.* **2018**, *28* (41), 1804128.
(40) Schulz, P.; Edri, E.; Kirmayer, S.; Hodes, G.; Cahen, D.; Kahn, A. Interface Energetics in Organo-Metal Halide Perovskite-Based Photovoltaic Cells. *Energy Environ. Sci.* **2014**, *7* (4), 1377–1381.
(41) Li, Y.; Feng, C.; Cheng, H.; Wang, Z.-S. $Zn_{0.8}Cd_{0.2}S$@PCBM Hybrid as an Efficient Electron Transport Layer for Air-Processed p-i-n Planar Perovskite Solar Cells: Improvement of Interfacial Electron Transfer and Device Stability. *Sol. RRL* **2018**, *2* (12), 1800222.
(42) Liu, G.; Zheng, H.; Xu, X.; Xu, S.; Zhang, X.; Pan, X.; Dai, S. Introduction of Hydrophobic Ammonium Salts with Halogen Functional Groups for High-Efficiency and Stable 2D/3D Perovskite Solar Cells. *Adv. Funct. Mater.* **2019**, *29* (47), 1807565.
(43) Abate, S. Y.; Huang, D.-C.; Tao, Y.-T. Surface Modification of $TiO_2$ Layer with Phosphonic Acid Monolayer in Perovskite Solar Cells: Effect of Chain Length and Terminal Functional Group. *Org. Electron.* **2020**, *78*, 105583.
(44) Sharma, A.; Singh, R.; Kini, G. P.; Hyeon Kim, J.; Parashar, M.; Kim, M.; Kumar, M.; Kim, J. S.; Lee, J.-J. Side-Chain Engineering of Diketopyrrolopyrrole-Based Hole-Transport Materials to Realize High-Efficiency Perovskite Solar Cells. *ACS Appl. Mater. Interfaces* **2021**, *13* (6), 7405–7415.

# *Supporting Information*

# Interface Passivation of Inverted Perovskite Solar Cells by Dye Molecules

*Yifang Qi[a], David Ndaleh[b], William E. Meador[b], Jared H. Delcamp[b], Glake Hill [a], Nihar Ranjan Pradhan[a], and Qilin Dai[a]**

a Department of Chemistry, Physics, and Atmospheric Sciences, Jackson State University, Jackson, MS, 39217, United States

b Department of Chemistry and Biochemistry, University of Mississippi, Oxford, MS, 38677, United States

* Corresponding author: Q. Dai, Email: *qilin.dai@jsums.edu*

Keywords: Inverted Perovskite, Cyanine dye, Charge transport, Interface, Stability

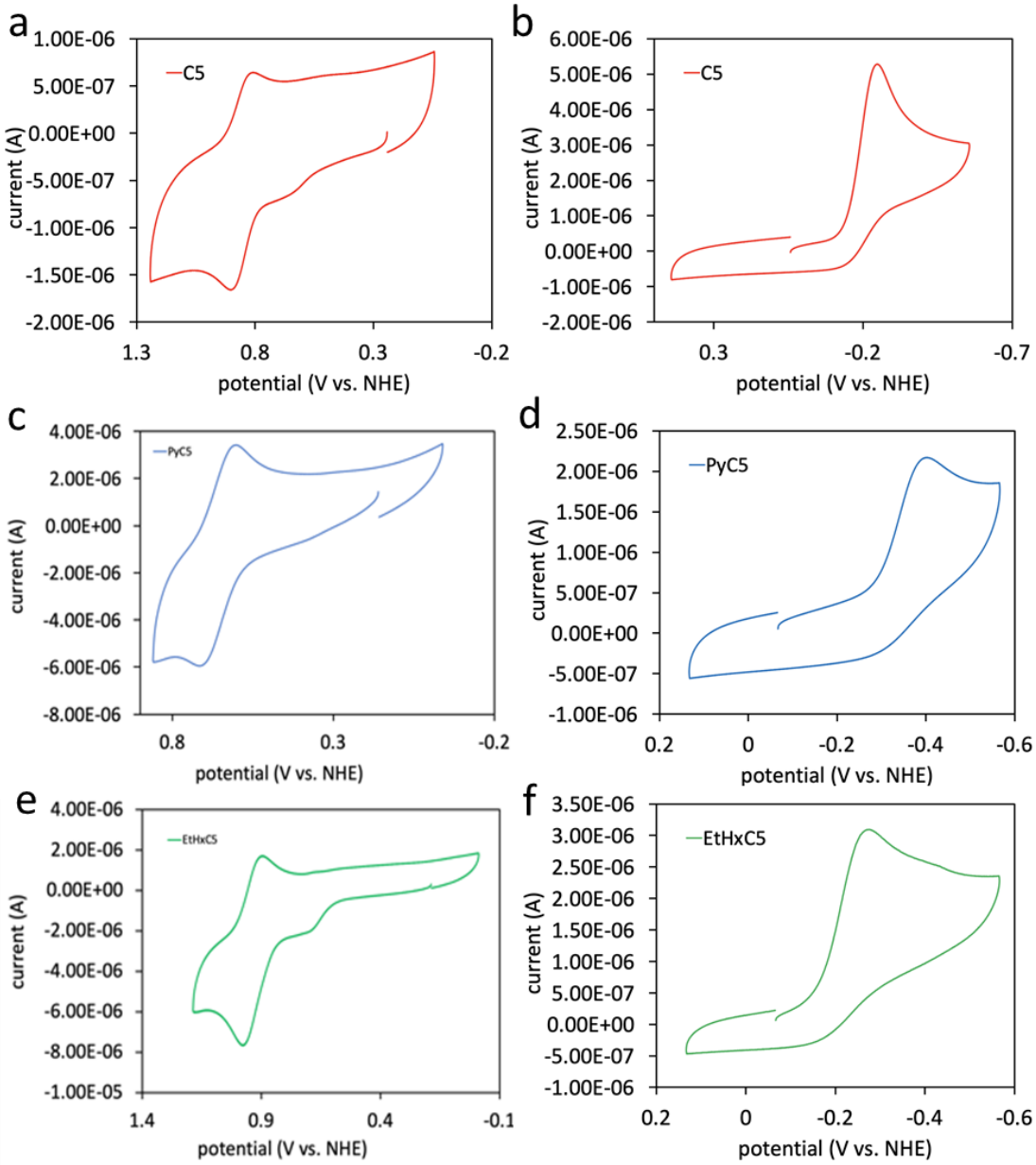


**Figure S1** a)-b) Cyclic voltammograms of Dye1 scanned in the positive and negative direction; c)-d) Cyclic voltammograms of Dye2 scanned in the positive and negative direction; e)-f) Cyclic voltammograms of Dye3 scanned in the positive and negative direction.

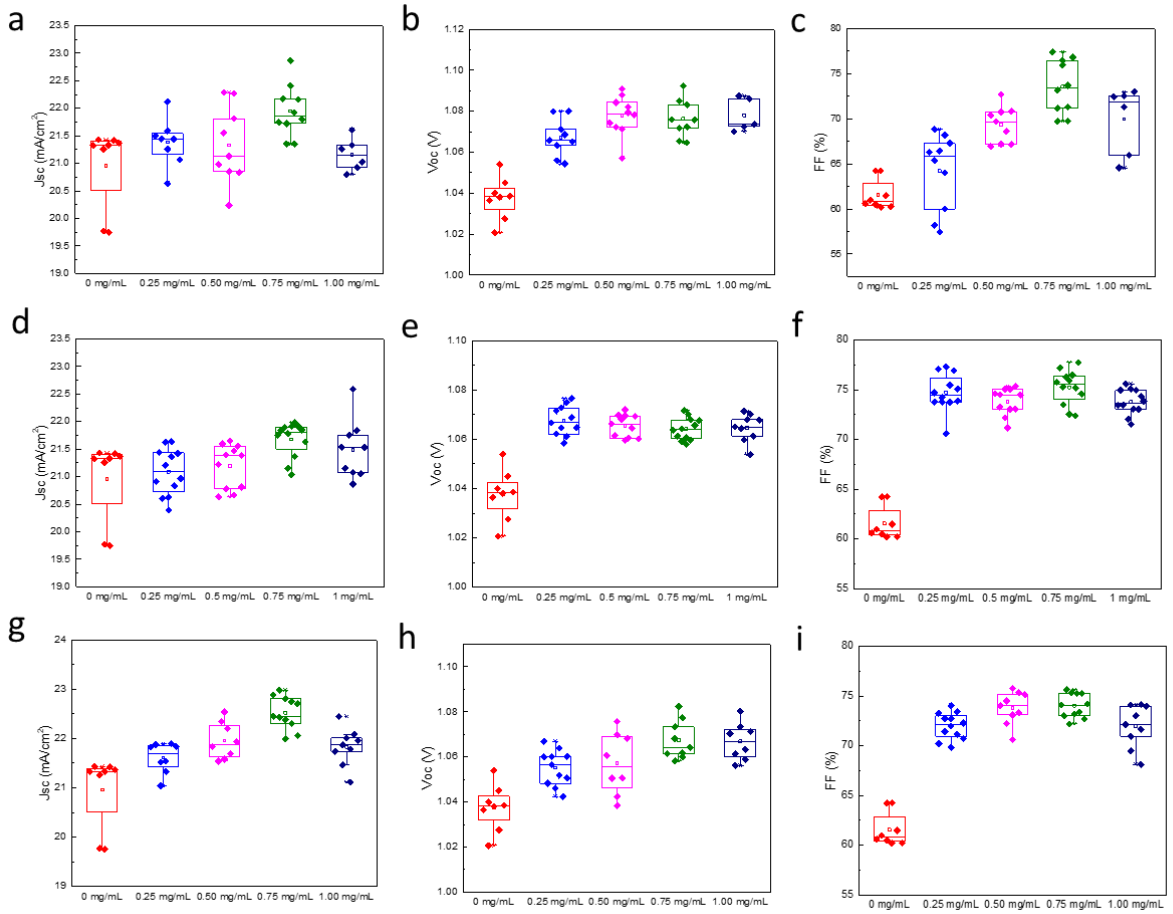


**Figure S2** a)-c) are the distributions of Jsc, Voc and FF of the devices with different Dye1 concentrations; d)-e) are the distributions of Jsc, Voc and FF of the devices with different Dye2 concentrations; g)-i) are the distributions of Jsc, Voc and FF of the devices with different Dye3 concentrations.